Effective Use of Focused Ion Beam (FIB) in Investigating Fundamental Mechanical Properties of Metals at the Sub-Micron Scale.

Julia R. Greer
Palo Alto Research Center (PARC)
3333 Coyote Hill Road, Palo Alto, CA 94304

ABSTRACT

Single crystal nano-pillars, ranging in diameter between 300 nm and 870 nm, were fabricated from epitaxial gold films on MgO substrates and subsequently uniaxially compressed. Flow stresses were found to strongly depend on sample size, as some of our smaller specimens were found to plastically deform in uniaxial compression at stresses as high as 800 MPa, ~50 times higher than for bulk gold. These high strengths are achieved via *dislocation starvation,* a regime where mobile dislocations have a higher probability of annihilating at a free surface than of multiplying and being pinned by other dislocations. Contrary to this, if dislocations are trapped inside by a coating, the strengthening mechanism is expected to be different. We compare plastic deformation of passivated and unpassivated single crystal gold nano-pillars and estimate the role of free surfaces. Preliminary results show that passivated samples achieve much higher stresses at equivalent sizes compared with the uncoated samples.

Keywords: *Focused Ion Beam (FIB); Nanoscale; Micromachining; TEM; Plasticity.*

1 INTRODUCTION

Recent advances in the two-beam focused ion beam (FIB) technology have enabled researchers to not only perform high-precision nanolithography and micro-machining, but also to apply these novel fabrication techniques to investigating a broad range of materials' properties at the sub-micron and nano-scales. In our work, the FIB is utilized in manufacturing of nano-pillars, as well as of TEM cross-sections to directly investigate plasticity of metals at these small length scales. In the last decade or so, the Focused Ion Beam has become one of the most widely used tools for sample fabrication, testing, and imaging [1-3]. This multidisciplinary tool is applicable to a broad range of projects like fabrication and testing of MEMS, sensors, micro-actuators, microfluidic devices, etc. With some care, FIB can be utilized in fabrication of intricate 3-D structures by both etching of the starting material and by deposition of metals from gas phase. One of the key contributions of FIB's availability for mechanical experiments is that it bridges the experimental length scale with the computational results, where sample sizes are generally specified in the number of atoms [4]. Until recently, mechanical deformation has largely been carried out in thin films either with or without substrates due to their relative ease of deposition and their industrial relevance. The development of the Focused Ion Beam (FIB) as a user-accessible fabrication tool has enabled constraining the specimens not only vertically but also in the in-plane directions. For example, an increasing number of research groups is studying size effects in plasticity by investigating fundamental mechanical deformation in micron- and sub-micron-sized pillars [5-9]. Although a unified theory explaining plasticity below a certain length scale remains a matter of great research and controversy, the results of most computational and experimental studies indicate an inevitable strength increase associated with the reduction in sample size, or a so-called size effect.

2 UNIAXIAL COMPRESSION

In this work, we focus our attention on size effects arising in uniaxial deformation of gold (FCC) nano-pillars with and without passivation on MgO substrates. We also compare their behavior to that of molybdenum (BCC) pillars, which are expected to strengthen through a different plasticity mechanism. The FIB is instrumental in nearly every step of these experiments, starting with pillar fabrication, micro-machining of the flat-punch indenter tip, and ending with machining TEM samples for dislocation activity investigation. The compressions were conducted in the DCM module of the MTS Nanoindenter XP, where a uniform top load was applied to the single-crystal samples of *sub-micron* dimensions, whose initial dislocation density was on the order of $10^{12}/m^2$ characteristic of a well-annealed metal. This particular type of deformation was chosen because the material is not expected to strengthen through one of the known mechanisms like strain gradient plasticity, dislocation confinement, grain size hardening, or initial lack of dislocations. The uniaxial compression procedure and methodology for stress-strain calculations, as well as the FIB fabrication technique are described in detail elsewhere [9]. An example of gold pillar on MgO substrate is shown in Figure 1(a). Gold pillars were fabricated from epitaxially-grown thin films on MgO substrates while Mo pillars were machined from single crystal bulk sample.

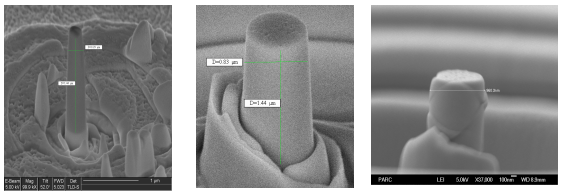

(a) (b) (c)

Figure 1. (a) 290-nm diameter single crystal gold pillar fabricated in the FIB on MgO substrate. (b)a representative Mo <001>-oriented pillar before compression, and (c)after severe compression. Initial diameter ~ 830 nm, final diameter after compression ~ 960nm.

A representative Mo pillar (initial diameter = 830 nm) before and after compression are shown in Figure 1(b,c). The final severe deformation state clearly shows that multiple slip systems were activated and that the compression was relatively homogeneous.

The experiments presented here are unique in their attempt to assess the effects of surfaces on the pillar strength as well as to compare plastic flow in FCC and BCC materials at nano-scale. While passivation of thin films is done routinely via sputtering or evaporation, uniform coating of complex geometries is much more challenging. The availability of Atomic Layer Deposition (ALD) for high-aspect ratio features is complementary to the FIB fabrication technique as it allows for studying the effects of passivation on the features of interest Key aspect of ALD is its utilization of sequential precursor gas pulses to deposit a film one layer at a time. The first precursor gas is introduced into the process chamber to produce a monolayer of gas on the substrate surface. The second precursor gas is then introduced into the chamber to react with the first gas on the surface of the substrate and to produce exactly a monolayer of film. Since each pair of gas pulses produces exactly one monolayer of film, the thickness can be precisely controlled.

3 DISCUSSION

3.1 Surface Effects

The results of our uniaxial compression experiments indicate a strong size effect: the flow stresses for gold pillars are much higher than the typical strength of bulk gold, estimated at 20 MPa at 2% strain. Moreover, the flow stresses for single-crystalline <001>-oriented pillars increase from ~50 MPa to 600 MPa as the diameter is reduced from 870 nm to 300 nm. Figure 2(a) shows the typical stress-strain curves for several *uncoated* nano-pillars, whose diameters varied from 300 nm to 870 nm. The methodology for stress calculation from the Nanoindenter-generated data is presented in detail elsewhere [9].

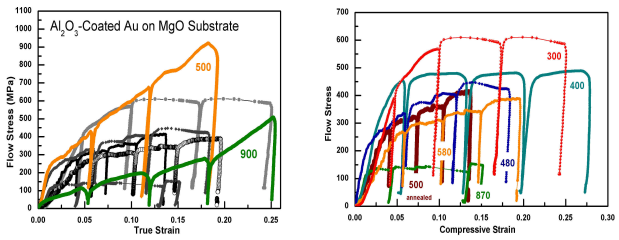

(a) (b)

Figure 2. Stress-strain curves generated from compression of sub-micron-sized gold nanopillars on MgO substrates. (a) All pillars were tested immediately after fabrication while the 500-nm diameter pillar was annealed prior to deformation. (b) Comparison of uncoated pillars (black) which exhibit virtually no strain-hardening at >10% strains vs. two alumina-coated pillars (colored) which show pronounced linear hardening.

An unusual feature of these curves is the near-saturation of the flow stress past ~ 10% strain, as it remains nearly constant upon further compression. This is consistent with the apparent lack of the Stage II strain-hardening region associated with the multiple dislocation cross-slip processes as their density increases. Contrary to this, the stress-strain behavior agrees more with the Stage I-type deformation, or the "easy glide" section of a low-symmetry oriented single crystal deformation curve. Moreover, the discrete slip events associated with the dislocation nucleation and glide are present in nearly every curve, with a larger number of slips in smaller-sized pillars. As reported earlier, the proposed hardening mechanism here is "hardening by dislocation starvation" where the mobile dislocations escape the crystal at an available free surface [9].

On the contrary, the alumina-coated pillars behave differently, as they exhibit conventional strain-hardening, with a higher hardening exponent for the smaller specimen size, as also shown by colored curves in Figure 2(b). Here, the curves for the uncoated pillars (black) are compared with those of the passivated pillars (colored). Not only do the coated pillars achieve higher strengths than their free-surface counterparts of equivalent sizes, but they also demonstrate a fundamentally different strengthening mechanism. Here, the dislocations are trapped inside the pillar by the outer layer, and hardening occurs through dislocation pile-ups within the pillar [10]. In order to estimate the role of the surface on the strength of the specimen, the results of three 500-nm diameter pillars with different surface treatments were compared. Figure 3 shows the stress-strain data for these specimens where the top-most curve corresponds to the pillar with alumina coating, and the open-circles and filled-circles curves represent the "as-FIB'd" and "post-FIB annealed" pillars, respectively.

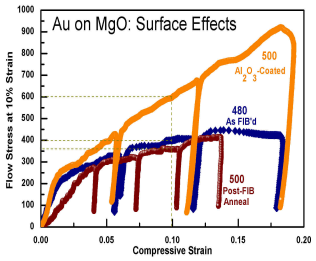

Figure 3. Stress vs. strain for 500-nm-diameter pillars. Stresses achieved by both "as-is" and annealed FIB pillars are similar to each other while the coated pillar is ~1.5x stronger.

This graph clearly demonstrates that a passivated 500-nm pillar continues strengthening throughout the compression, achieving its maximum stress of ~900 MPa at 20% strain. The coated pillar attains ~1.5X higher stresses at 10% strain than the uncoated pillars and experiences a significant amount of linear strain-hardening, with the slope of ~4 GPa, which is absent in the uncoated pillars. Unlike the passivated sample, the stresses of the annealed and unannealed pillars achieve similar levels between 350 MPa and 500 MPa and remain nearly constant upon further compression. This suggests that dislocation nucleation stresses required to generate new dislocations from surface steps in the uncoated pillars are lower than those required to move them through the dislocation forest.

3.2 FCC vs. BCC: Plasticity Comparison

The testing methodology and stress calculations for nano-pillars in uniaxial compression are based on the author's previous work, which is fully described in [9]. The axial stress was calculated by dividing the imposed load by the plastic area determined based on conservation of plastic volume. In order to provide a fair comparison between the strengths in BCC and FCC materials, the *shear stress* resolved on the appropriate slip plane was calculated by multiplying the axial stress by the Schmid factor. Figure 4 shows the resolved shear stress-shear strain curves generated based on the experimental load-displacement data collected by the Nanoindenter.

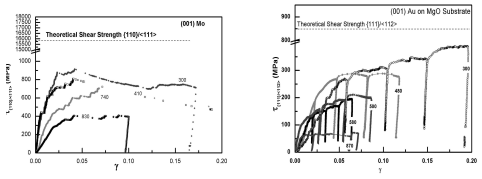

(a) (b)

Figure 4. Stress vs. strain for (a) Mo and (b) Au nano-pillars. Gold pillars were intentionally unloaded and re-loaded several times throughout the experiment. Numbers adjacent to each curve represent the initial diameter of the pillar.

The molybdenum pillars were compressed without intentional unloading in the middle of the experiment while the gold pillars were unloaded and re-loaded several times before reaching its final strain. It is clear from the two sets of curves that at 5 % strain, a 300-nm Mo nano-pillar reaches the shear stress of 908.1 MPa compared with 274.6 MPa for Au at equivalent strain. This is expected since BCC metals exhibit high Peierls stresses, or lattice resistance to dislocation motion. At the same time, density functional theory (DFT) predicts that the ideal shear strength of Au on its slip plane is 850 MPa and that for Mo is 1518 MPa [11]. This means that the 300-nm Au pillar achieves ~32% of its theoretical strength while the strongest Mo pillar in our experiment (also 300-nm diameter) reaches only 6% of its theoretical strength. Due to slight misalignment in the initial stages of deformation, we chose to compare flow stresses at 5% strain, when full contact is established, rather than yield stresses, which cannot be unambiguously defined here. Figure 5 shows the scaling behavior of Au and Mo pillars in terms of the resolved shear stress at 5 % strain vs. pillar diameter and shows that while the scaling law has a power form for both types of crystals, its scaling exponents are different by nearly a factor of 2.

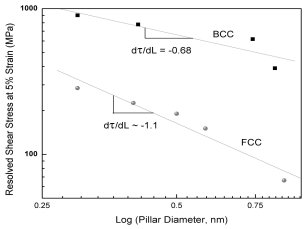

Figure 5. Resolved shear stress vs. size (diameter) for Au (FCC) vs. Mo (BCC). The power exponents of -0.68 and -1.1 suggest fundamentally different dislocation evolution mechanisms.

The relative increase of plastic strength at smaller diameters seems to be less pronounced for BCC metals compared with FCC metals. The 38% difference in the power law exponents suggests that different dislocation mechanisms are operating in FCC and BCC pillars. To gain further insights into the origins of the observed size dependence, Dislocation Dynamics (DD) simulations in elastic cylinders with dislocations described by different mobility functions to mimic their behavior in FCC and BCC metals are performed and reported elsewhere [12].

REFERENCES

[1] K. S. H. Hosokawa, Y. Chino, Y. Yamada, C. E. Wen and M. Mabuchi, Materials Science and Engineering A 344 (2003) 365-367.

[2] S. J. Kim, Yamashita, T., Nagao, M., Sato, M., Maeda, H., Japanese Journal of Applied Physics 41 (2002) 4283-4286.

[3] J. H. M. Daniel, D.F. Walker, J.F., Engineering Science and Education Journal 7 (1998) 53-56.

[4] J. R. Greer, Reviews on Advanced Materials Science 13 (2006) 59-70.

[5] B. E. Schuster, Wei, Q., Zhang, H., Ramesh, K.T., Applied Physics Letters 88 (2006) 103112-103111-103113.

[6] H. Zhang, Schuster, B.E., Wei, Q., Ramesh, K.T., Scripta Materialia 54 (2005) 181-186.

[7] M. D. Uchic, Dimiduk, D.M., Materials Science and Engineering A 400-401 (2005) 268-278.

[8] V. S. Deshpande, Needleman, A., Van der Giessen, E, Journal of the Mechanics and Physics of Solids 53 (2005) 2661-2691.

[9] J. R. Greer, Oliver, W.C., Nix, W.D., Acta Materialia 53 (2005) 1821-1830.

[10] Y. X. L. Nicola, J.J. Vlassak, E. Van der Giessen, A. Needleman, Journal of the Meechanics and Physics of Solids 54 (2006) 2089-2110.

[11] S. Ogata, J. Li, N. Hirosaki, Y. Shibutani, S. Yip, Phys. Rev. B **70** (2004).

[12] J.R. Greer, C. Weinberger, W. Cai, TMS Proceedings, 2007 (Orlando, Fl).